

Two-magnon Raman scattering in $A_{0.8}Fe_{1.6}Se_2$ systems: competition between superconductivity and antiferromagnetic order

A. M. Zhang, J. H. Xiao, Y. S. Li, J. B. He, D. M. Wang, G. F. Chen, B. Normand, and Q. M. Zhang
Department of Physics, Renmin University of China, Beijing 100872, P. R. China

T. Xiang

*Institute of Physics, Chinese Academy of Sciences, Beijing 100190, P. R. China and
Institute of Theoretical Physics, Chinese Academy of Sciences, P.O. Box 2735, Beijing 100190, P. R. China*

(Dated: April 26, 2022)

We have performed Raman-scattering measurements on high-quality single crystals of $A_{0.8}Fe_{1.6}Se_2$ superconductors of several compositions. We find a broad, asymmetric peak around 1600 cm^{-1} (200 meV), which we identify as a two-magnon process involving optical magnons. The intensity of the two-magnon peak falls sharply on entering the superconducting phase. This effect, which is entirely absent in the non-superconducting system $KFe_{1.5}Se_2$, requires a strong mutual exclusion between antiferromagnetism and superconductivity arising from proximity effects within regions of microscale phase separation.

PACS numbers: 74.70.-b, 74.25.Kc, 63.20.kd, 78.30.-j

I. INTRODUCTION

The investigation of iron-based superconductors experienced an exciting breakthrough in the synthesis of arsenic-free, potassium-intercalated FeSe.¹ This material has a maximum $T_c = 32\text{ K}$, which is duplicated on replacing K by other monovalent ions, including Rb, Cs, and Tl (denoted henceforth by A).² These systems are found to be non-stoichiometric both in A and in Fe content, and numerous studies have been performed which identify ordered structures of the vacancies in the Fe plane. Long-range magnetic order appears to be involved implicitly in the selection of the ordered vacancy pattern, which leads directly to the most anomalous property of the $A_xFe_{2-y}Se_2$ systems, namely the apparent coexistence of antiferromagnetism and superconductivity.

The initial suggestion of Fe vacancy order came from transmission electron microscopy (TEM)³ and X-ray diffraction (XRD).⁴ Both infrared⁵ and Raman⁶ measurements observed many more phonon modes than would be expected for stoichiometric Fe superconductors, such as the $BaFe_2As_2$ (“122”)⁷ or $Fe(Se,Te)$ (“11”) structures.⁸ These were shown^{6,9} to be consistent with the $\sqrt{5}\times\sqrt{5}$ Fe-vacancy pattern expected for an Fe content of 1.6. This low-temperature structure was then demonstrated conclusively by neutron diffraction studies of several crystals.¹⁰ However, other Fe-vacancy structures have also been observed in $A_xFe_{2-y}Se_2$, with neutron diffraction revealing not only the $\sqrt{5}\times\sqrt{5}$ phase ($I4/m$) but also a vacancy-disordered ($I4/mmm$) phase above 500 K and a $\sqrt{2}\times\sqrt{2}$ phase ($Pmna$) below 500 K.¹¹ Experiments by scanning tunneling microscopy (STM), TEM, X-ray, and neutron scattering have suggested the possibility that superconductivity may also be present in the $\sqrt{2}\times\sqrt{2}$ phase.¹²

Still more anomalous is that the ordered $\sqrt{5}\times\sqrt{5}$ Fe-vacancy structure is not only accompanied by, but

to a significant extent stabilized by, a very strong antiferromagnetic (AF) order.¹⁰ Setting in at a remarkably high transition temperature around 520 K, the spin order consists of AF-coupled four-site ferromagnetic blocks, with large on-site moments of $3.3\mu_B$. The transition was confirmed by high-temperature bulk magnetic measurements¹³ and the large moment by Mössbauer spectroscopy,¹⁴ while muon spin rotation (μ SR) experiments put the magnetic volume fraction at 90–95%.¹⁵ In addition, inelastic neutron scattering (INS)¹⁶ and two-magnon Raman measurements (below) also show the presence of a strongly magnetic phase. However, nuclear magnetic resonance (NMR) experiments¹⁷ find singlet superconductivity with only weak AF fluctuations, and no detectable magnetic order. No evidence of magnetic order is present in the Fermi surfaces observed by angle-resolved photoemission spectroscopy (ARPES).¹⁸ Both of these results suggest that the presence of magnetic order and superconductivity in the $A_xFe_{2-y}Se_2$ superconductors should be the result of a macroscopic phase separation rather than any type of microscopic coexistence or cohabitation.

The question of coexistence has recently been the focus of the most intense experimental investigation. A clear consensus has emerged in favor of phase separation, which has been reported in optical¹⁹ and ARPES measurements.²⁰ Specially designed Mössbauer,²¹ X-ray,²² and in-plane optical spectroscopic measurements²³ have all been used to specify that the phase separation occurs on nanoscopic length scales, and this has now been observed directly by STM on epitaxially grown films.²⁴ Some of these authors^{20,24} have further identified that vacancy order is a property only of the AF phase, while the superconducting phase is uniform and may be composed of stoichiometric AFe_2Se_2 regions, a conclusion also suggested by INS.²⁵ However, none of these works has shed any light on the coupling of the two phases, by which is meant the key question of whether superconductivity

and antiferromagnetism can merely exist side by side, or whether they also influence each other.

In this paper, we answer this question by using Raman scattering to measure the high-energy excitations in three superconducting (SC) $A_{0.8}Fe_{1.6}Se_2$ samples and one non-SC $KFe_{1.5}Se_2$ crystal. We observe broad two-magnon scattering signals whose energy demonstrates a common origin in the optical magnon modes of the complex unit cell. Strikingly, the continuous increase of the two-magnon intensity with decreasing temperature ends abruptly at T_c in the SC systems, displaying a rapid drop at $T < T_c$. Our results demonstrate the intrinsic opposition of superconductivity to bulk magnetism. They also add to the weight of evidence that the size of the cohabitating regions of AF order and superconductivity in the $A_{0.8}Fe_{1.6}Se_2$ materials is microscopic.

The structure of the manuscript is as follows. In Sec. II we introduce the materials and the experimental techniques employed. Section III presents our primary results for two-magnon Raman scattering, discussing the broad signal we observe in all samples, its origin, polarization-dependence, and a fine structure of subpeaks. The temperature-dependence of our results is so remarkable that it merits a separate section, Sec. IV, where we quantify the sharp drop below T_c by means of intensity integrations. In Sec. V we discuss the consequences of our observations for models of cohabitation between magnetism and superconductivity. A short summary can be found in Sec. VI.

II. MATERIALS AND METHODS

The FeSe-based single crystals used in our measurements were grown by the Bridgman method,²⁶ and were cleaved from exactly the same batch as those used in neutron scattering experiments by Bao *et al.*^{10,11} The stoichiometry of each crystal is determined by inductively coupled plasma atomic emission spectroscopy (ICP-AES) and by neutron diffraction refinement.¹⁰ Thus we identify our SC samples as $K_{0.8}Fe_{1.6}Se_2$ ($T_c = 32$ K), $Tl_{0.5}K_{0.3}Fe_{1.6}Se_2$ ($T_c = 29$ K), and $Tl_{0.5}Rb_{0.3}Fe_{1.6}Se_2$ ($T_c = 31$ K), while the non-SC crystal is $KFe_{1.5}Se_2$. XRD analysis shows no discernible secondary phase in any of the crystals. Their resistivities and magnetizations were measured respectively with a Quantum Design physical properties measurement system (PPMS) and the PPMS vibrating sample magnetometer (VSM). Both quantities exhibit sharp SC and diamagnetic transitions for all three samples (shown below, in the insets of Fig. 2), proving the high quality of the crystals used in our Raman investigation. Magnetization measurements were performed both before and after the Raman investigation, confirming that no changes in the SC state occur during our experiments.

Before performing a high-energy Raman measurement, we first cleaved a piece of crystal (approx. $1 \times 2 \times 0.2 \text{ mm}^3$) in a glove box to obtain a flat, shiny (*ab*)-plane surface.

The freshly-cleaved crystal was sealed under an argon atmosphere and transferred rapidly into the cryostat, which was evacuated immediately to 10^{-8} mbar. We use a pseudo-backscattering Raman configuration with a triple-grating monochromator (Jobin Yvon T64000). All of the Raman spectra were collected with a 532 nm solid-state laser (Torus 532, Laser Quantum), except for the spectrum in Fig. 1(b), where a 633 nm Melles Griot He-Ne laser was used to exclude the possibility of photoluminescence effects (Sec. III). The beam is focused to a spot diameter of 20 μm at the sample surface and its power reduced below 0.5 mW at low temperatures. The temperature in the spot is calibrated from the Stokes and anti-Stokes spectra.

The T64000 spectrometer works in subtractive mode. The third-stage grating, which has 1800 grooves per mm, has a resolution of approximately 0.6 cm^{-1} . Each spectral window covers 400-600 cm^{-1} . Because our spectrometer is not equipped with a low-density grating, we measure a “long” spectrum of the types shown in Secs. III and IV by combining several short spectral windows. These windows can be joined smoothly because the stray-light level is negligible at the high wavenumbers we probe. Long spectra from 600 to 3920 cm^{-1} were obtained by combining seven spectral windows. The combination quality is high due to the high quality of the cleaved crystal surface, which allows a precise determination of the relative spectral intensity.

This procedure is accurate for the shapes of broad features. At times when we found the intensities to have an error of a few percent, we took additional steps to suppress their fluctuations. The most fundamental was to repeat our measurements, which was particularly important around T_c (Sec. IV), and where we performed three or more sets of scans in order to obtain a completely reproducible spectrum at each temperature. Another step was to merge the high-energy tails, as these should depend only on “extrinsic” factors (such as the geometry, the surface, and the instrument) rather than on intrinsic materials properties. If the tails did not merge automatically, the whole spectrum was multiplied by an overall factor to ensure a match. We also normalized the low-energy spectra using a Bose-Einstein thermal factor, and this led to very close agreement between spectral segments in almost all cases. Because the low-energy spectra lie rather close to the laser line, they have a higher possibility of being contaminated by stray light, and thus we took both the high- and low-energy spectra as criteria to guarantee that each spectrum is collected with the correct relative intensity.

III. TWO-MAGNON RAMAN SCATTERING

In Raman scattering by magnetic excitations, the dominant contribution is given by two-magnon processes involving spin excitations of equal and opposite momenta close to the zone boundary. This is the origin of the well-

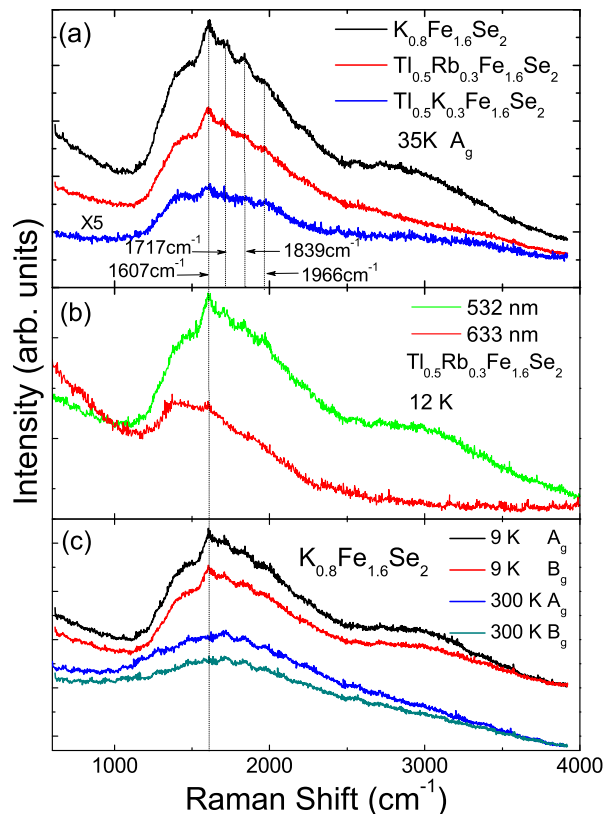


FIG. 1: (Color online) (a) Raman spectra for the three SC samples measured at 35 K in the A_g channel. Dotted lines mark peak frequencies observed in all samples. (b) Comparison of Raman spectra measured with excitation wavelengths of 633 nm (red) and 532 nm (green). (c) Similar two-magnon spectra are observed in both A_g and B_g channels.

defined peak at energies $\omega \approx 3J$ in square-lattice AF structures,²⁷ which has been widely exploited in cuprate superconductors despite a strong broadening of the signal due to AF spin fluctuations.²⁸ Because the penetration depth for a Raman measurement is up to 100 nm in typical systems with lower carrier densities, this can be regarded as a bulk rather than a surface technique. Thus Raman scattering plays an essential role in studying magnetism in correlated electron systems. For Fe-based superconductors, the only two-magnon measurements reported to date are for the 122 and 11 systems.²⁹

A. Sample characteristics

Figure 1(a) shows the Raman spectra of the three SC samples, measured to 4000 cm^{-1} at 35 K. All three samples show a broad and asymmetric peak around 1600 cm^{-1} (200 meV), while some also suggest a high-energy shoulder at $2800\text{--}3500 \text{ cm}^{-1}$. The most remarkable feature is that all three spectra are qualitatively identical, proving that the measured behavior is truly intrinsic to the FeSe layers. While the signal intensities vary with

the A-site dopant, whose non-stoichiometry leads to clear disorder effects, these are arbitrary units. As in any Raman measurement, they depend strongly both on the sample (at fixed composition) and on the chosen spot on each sample. For this reason, in the remainder of manuscript we focus on the energetics of the scattering response, which are read from the Raman shift, and on relative intensities only within a single measurement.

Before proceeding further, in Fig. 1(b) we compare the spectra obtained in one sample with two different excitation wavelengths, 633 nm and 532 nm. While the background terms are clearly different, the broad feature around 1600 cm^{-1} is certainly reproduced at 633 nm, albeit with a global intensity reduction. In fact a similar reduction effect is also observed in studying two-magnon processes in cuprates.³⁰ This comparison confirms that the 1600 cm^{-1} feature is indeed a real Raman signal, and not a photoluminescence effect. In contrast, the possible high-energy shoulder around 3000 cm^{-1} is not present when excited by a 633 nm laser, which suggests very strongly that it is due to photoluminescence, rather than to an intrinsic process.

We also comment briefly on a polarization analysis of our spectra. The symmetry-dependence of the two-magnon signal is shown in Fig. 1(c). The peaks measured in the A_g and B_g channels show similar lineshapes and only small differences in intensity. This behavior is quite different from the cuprate superconductors, where two-magnon processes are allowed only in the B_{1g} channel, and arises because the $\sqrt{5} \times \sqrt{5}$ vacancy-ordered structure lowers the lattice symmetry of the $A_{0.8}\text{Fe}_{1.6}\text{Se}_2$ materials. The presence of a two-magnon signal in both channels has been demonstrated in local-moment models for Fe-based superconductors in Ref. [31].

B. Optical magnons

The origin of the primary spectrum is indisputably magnetic: optical phonon modes appear only below 300 cm^{-1} ,^{5,6} and high-order multi-phonon processes may be safely excluded. An electronic origin in inter-band transitions is excluded by an absence of 200 meV features in angle-resolved photoemission spectroscopy (ARPES).¹⁸ To understand the magnetic contributions, we consider³² the magnon bands of the $\sqrt{5} \times \sqrt{5}$ magnetic structure [Fig. 2(a)]. These bands consist of one acoustic branch, which corresponds to processes involving the effective block spin of each four-site unit, accompanied by three optical branches arising from local processes on the square lattice of Fe sites. They are shown schematically in Fig. 2(b), where the energy scales are motivated by an inelastic neutron scattering (INS) study of the magnetic excitations in $\text{Rb}_{0.89}\text{Fe}_{1.58}\text{Se}_2$.¹⁶ This investigation suggested that the acoustic branch extends to 70 meV, while two rather flat optical branches are present at 110–120 meV, accompanied by a high-lying optical branch around 200 meV.

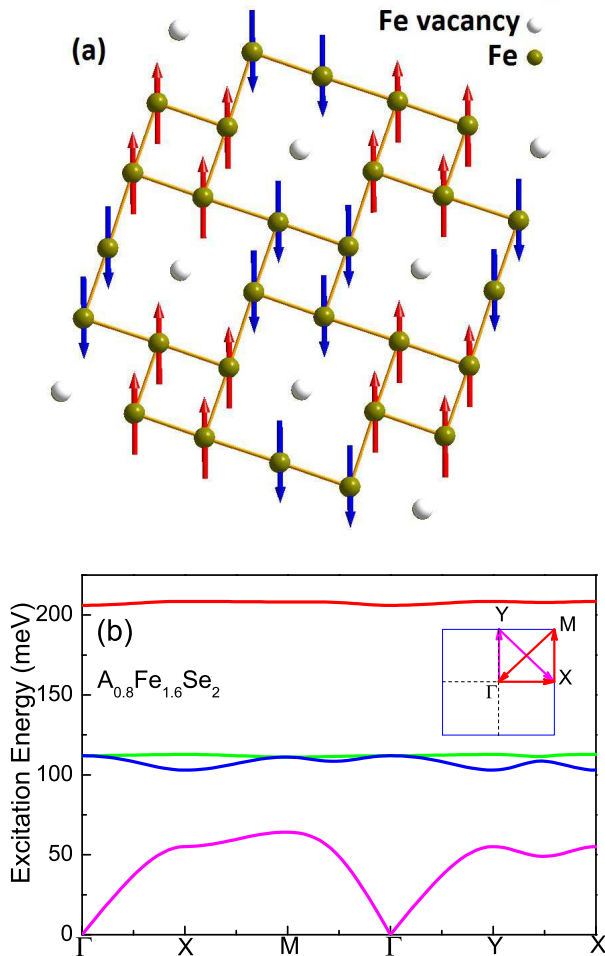


FIG. 2: (Color online) (a) Schematic representation of the $\sqrt{5} \times \sqrt{5}$ vacancy-ordered structure and magnetically ordered configuration of the $\text{Fe}_{1.6}\text{Se}_2$ plane. (b) Corresponding magnon band structure; the four-site unit cell results in four magnon bands, of which one is acoustic and the remaining three are optical. With this parameter choice, which is based on the INS results of Ref. [16], the dominant contributions to the two-magnon Raman intensity are due to this optical modes at 110–125 meV (shown in blue and green); we caution that some alterations to the parameter set may be required to account for the absence in our measurements of a high-lying optical mode.

In a local picture of two-magnon Raman scattering, the dominant energy scale is given by reversing the spins on the shortest bond(s), in the system. The magnetic exchange constants within the Fe plane estimated in Ref. [16] give an energy of order 220 meV, on both nearest- and next-neighbor bonds. This is exactly the peak energy we observe. Such local processes are contained in the optical magnon bands, and therefore our primary signal may be ascribed to two-magnon processes involving the 110–120 meV optical magnons of Ref. [16]. One-magnon signals, which would be expected at 800–900 cm^{-1} , appear to be small. We do not ob-

serve significant contributions from the acoustic magnon branch. Our results also do not provide a reliable indication for the presence of a high-lying optical magnon mode (the 3000 cm^{-1} feature reported by INS), and therefore we use the exchange constants of Ref. [16] for illustration only. Finally, the breadth in frequency of the signal we observe is strongly reminiscent of cuprates, and it cannot be explained solely on the basis of multiple magnon bands; it constitutes clear evidence for strong spin-fluctuation effects occurring in the FeSe planes of the $\text{A}_{0.8}\text{Fe}_{1.6}\text{Se}_2$ materials.

C. Fine Structure

The two-magnon intensity [Fig. 1(a)] also contains several individual peaks superposed on the broad, two-magnon signal, occurring at 1607, 1717, 1839, and 1966 cm^{-1} . These apparent resonances are small in intensity and rather narrow in energy. Their location and regular spacing are completely reproducible between the different superconducting samples, adding strongly to the evidence that all of the features of our observed response are characteristic of the FeSe planes.

We do not yet have a complete explanation for these features. Although the majority of our measured intensity is a two-magnon signal, in our calculated Raman response we have not been able to reproduce these features on the basis of the magnon band structure of Ref. [16]. Even mode dispersions as flat as the magnon bands appearing between 110 and 125 meV in Fig. 2(b) do not have density-of-states effects (arising from their upper and lower band edges) sufficiently strong that peaks of this sharpness can emerge. The regularity of the peak spacings is also difficult to reproduce.

Another possibility would be the “two-magnon plus phonon” processes proposed to explain sharp features in the two-magnon Raman response of cuprates.^{33,34} By this mechanism, the phonon or phonons act(s) to lower the symmetry of the net two-magnon absorption process, and its wave vector allows contributions from many more pairs of magnon wave vectors. In the context of cuprates, particularly strong additional contributions were obtained from in-plane $(\pi, 0)$ phonons involving the O atoms. While analogous processes in the FeSe plane are more difficult to isolate because of its buckled structure (the Se atoms are located alternately above and below the Fe plane), we do have, from our own previous results for Raman scattering by phonons in $\text{K}_{0.8}\text{Fe}_{1.6}\text{Se}_2$,⁶ a rather complete accounting of the available vibrational modes. We found experimentally that the most intense phonon modes lie at energies of 135, 203, and 265 cm^{-1} . All have A_g symmetry and we were able theoretically to show that all three involve predominantly c -axis motions of the Se atoms. Further microscopic analysis is required of whether different combinations of phonon excitations on the intervening Se atom during the local spin-flip process can enhance the creation of magnon pairs.

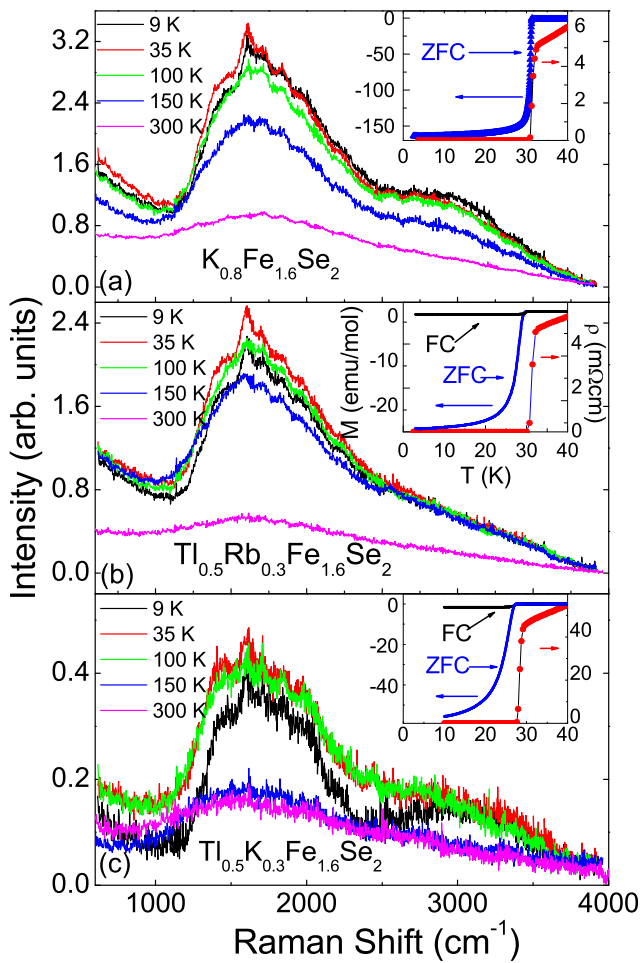


FIG. 3: (Color online) Two-magnon scattering intensity in the three SC crystals at selected temperatures. Intensities at 35 K (red) are higher than those in the SC state (black). Insets: resistivity and magnetization data at and below T_c .

IV. TEMPERATURE-DEPENDENCE

In Fig. 3 we show the two-magnon signals for all three SC samples over a range of temperatures. Lowering the temperature causes the peaks to become sharper and their intensity to rise continuously, as expected from a reduced thermal scattering of magnons. Remarkably, this tendency is interrupted at T_c . For the spectra in Fig. 3(a), the intensity in the SC state (9 K) clearly lies below that in the normal state near T_c (35 K) at frequencies below the peak, and then lies on or slightly above it. This behavior is not ambiguous in Fig. 3(b), where the low-temperature signal lies below the normal-state one everywhere. Finally, the difference is quite dramatic in Fig. 3(c), although the data here are noisier.

To place this result in perspective, we show in Fig. 4 the corresponding spectra for the non-SC sample, measured to 5300 cm^{-1} . While higher temperatures suppress the intensity more strongly than for the SC samples, at low temperatures there is no reverse: sharper modes de-

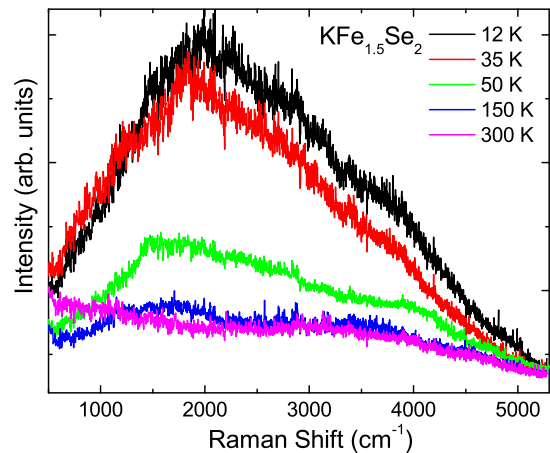


FIG. 4: (Color online) Temperature-dependence of the Raman intensity in non-superconducting $\text{KFe}_{1.5}\text{Se}_2$.

liver a more intense signal. Even in underdoped cuprates, where there are many reports of coexisting magnetism and superconductivity, and there is little debate that the charge carriers and magnetic moments arise from the same electrons, we are unaware of any reports of such a phenomenon in two-magnon Raman spectra.

We quantify the change in spectra around T_c by integrating the measured intensities over the two-magnon peak. We adopt three different definitions of the integration window in order to gain the maximum understanding of the significance of our results. These are a) integration over the entire range from 600 to 3920 cm^{-1} ; b) choosing the window from 1100 to 2600 cm^{-1} to focus on the signal arising from the 110 – 120 meV optical magnons; c) following the method of Blumberg *et al.*,³⁵ who defined the integrated two-magnon peak intensity as the excess signal above the minima on either side of the peak, which defines a type of background-free contribution between (in our system) 1100 and 2500 cm^{-1} . These integration areas are represented in the respective panels of Fig. 5.

In a further attempt to minimize extraneous effects, we chose to focus on our sample of $\text{Tl}_{0.5}\text{Rb}_{0.3}\text{Fe}_{1.6}\text{Se}_2$ [Fig. 3(b)]. In our sample of $\text{K}_{0.8}\text{Fe}_{1.6}\text{Se}_2$ [Fig. 3(a)], the ratio of integrated intensities between T_c and 9 K does not show a strong effect [by method (b), $I^b(35)/I^b(9) = 1.02$], but noisy integrated intensity data as a function of temperature led us to doubt the overall reliability of this sample, due to its age and to complications with surface light reflections. By contrast, in our sample of $\text{Tl}_{0.5}\text{K}_{0.3}\text{Fe}_{1.6}\text{Se}_2$ [Fig. 3(c)] we obtain $I^b(35)/I^b(9) = 1.30$, suggesting a massive reduction effect; we discount this data due to its significantly lower overall intensity and consequently higher signal-to-noise ratio (Fig. 1). For our sample of $\text{Tl}_{0.5}\text{Rb}_{0.3}\text{Fe}_{1.6}\text{Se}_2$, we measured high-frequency Raman spectra over a range of narrowly spaced temperature points. The integrated intensities derived from our data for all three definitions in the previous paragraph are presented in Fig. 5. All show a steady increase with decreasing temperature above T_c , terminated

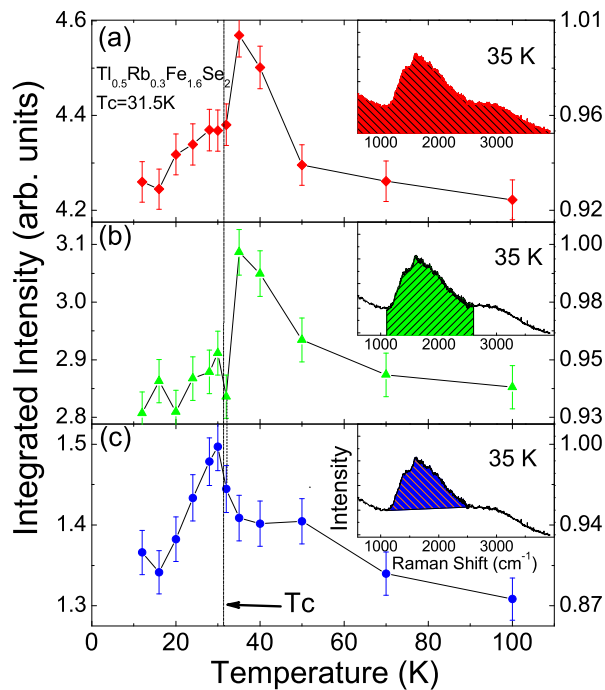


FIG. 5: (Color online) Temperature-dependence of the integrated scattering intensity for $\text{Tl}_{0.5}\text{Rb}_{0.3}\text{Fe}_{1.6}\text{Se}_2$. Insets: the shaded regions represent the integration area used in each panel. (a) Integration over the full measurement frequency range 600–3920 cm^{-1} without background subtraction. (b) Integration over the primary two-magnon contribution between 1100 and 2600 cm^{-1} without background subtraction. (c) Integration between the peak minima following Ref. [35], which corresponds to a frequency range 1100–2500 cm^{-1} and the subtraction of a background term.

by a sharp drop occurring essentially at T_c . This drop appears to be continuous, as the rapid opening of the superconducting gap at T_c acts to remove weight from the two-magnon intensity. The lost weight then saturates as the gap approaches a constant value at lower temperatures. Depending on the definition of the integration region, this loss of weight is a 5–10% effect.

V. DISCUSSION: COMPETITION

The two-magnon Raman intensity reflects directly a magnetic order. We have confirmed the presence of superconductivity both before and after our Raman measurements. The loss of intensity at and below T_c is therefore a clear statement concerning the coupling and the intrinsic opposition of superconductivity and antiferromagnetism.

The mutual interaction of magnetism and superconductivity has been difficult to investigate. While μSR is the most accurate local probe for estimating the magnetic volume fraction of a system, the technique gives no information on the SC state. Neutron diffraction stud-

ies have found that the intensity of the (101) magnetic Bragg peak seems to show a sudden saturation at $2T_c$.¹⁰ In Mössbauer measurements, a change in hyperfine field below T_c is suggested, but is not detected clearly.¹⁴ By contrast, our results do demonstrate clearly the nature of the relationship. Because we observe a 5-10% effect in a system which may be little more than 5-10% superconducting by volume fraction, we conclude that superconductivity and magnetism share a strong mutual exclusion.

Within the framework of microscale phase separation discussed in Sec. I, one possible scenario for the strong competition we observe between superconductivity and AF order is a true, microscopic coexistence in the magnetic phase. This would require that the superconductivity be a bulk property not only of the paramagnetic (PM) phase observed by NMR and ARPES, but also of the AF phase. However, band-structure calculations³⁶ have shown this phase to be a semiconductor, and this scenario would require that it could become weakly metallic due to non-stoichiometry-induced doping. The predicted energy gap to the conduction bands makes this possibility unlikely. Further, it remains to be understood how a system with such strong magnetism ($T_N = 520$ K) could simultaneously host such strong superconductivity ($T_c = 32$ K). One year of intensive investigation into the $\text{A}_x\text{Fe}_{2-y}\text{Se}_2$ materials has not yet revealed any qualitatively different properties to justify discarding the conventional understanding concerning generic exclusion of magnetism and superconductivity.

The alternative scenario relies on microscale phase separation. In this case, the superconductivity is a property of the PM phase alone, but this phase must be percolating, despite its small volume fraction, for the system to be a bulk superconductor. The measured volume fractions thus suggest a system of microscopic magnetic domains, whose disordered boundary regions are the PM phase. When the latter turn superconducting, they are required to drive a large fraction of the magnetic volume superconducting by proximity, reducing the ordered moment by the 5–10% that we observe. Such a physical proximity effect necessitates large contact areas between the AF and PM regions, and hence our results confirm that the lengthscale of the phase separation is required to be nanoscopic. Taken together with all of the other experimental evidence for nanoscale phase separation (Sec. I), we conclude that the microscopic mechanism for the strong competition we observe between magnetic order and superconductivity is an extensive grain-boundary proximity effect.

For completeness, we conclude this discussion by excluding two further scenarios. Because our Raman phonon measurements contain no evidence, in the form of phonon anomalies, for any type of structural phase transition near T_c ,⁹ an explanation for our results in terms of changes in the magnetism of the AF phase is excluded. Because our experiments probe many hundreds of atomic layers, and indeed possibly complete domains of the mag-

netic structure, they cannot be the consequence of a surface phenomenon.

VI. CONCLUSION

In summary, we have measured the high-energy Raman-scattering intensity in three different $A_{0.8}Fe_{1.6}Se_2$ superconductors. We find a robust and reproducible signal in all cases, which can be ascribed to two-magnon scattering processes involving the optical magnons of the $\sqrt{5} \times \sqrt{5}$ magnetic structure. We have discovered a striking drop in two-magnon Raman intensity below T_c , which has no precedent in other strongly correlated electronic superconductors. The magnitude of this competitive effect suggests an almost complete mutual exclusion of superconductivity and magnetic order due to proximity effects occurring within a microstructure based on nanoscopic phase separation.

Acknowledgments

We thank T. Li, Z. Y. Lu, and W. Bao for helpful discussions. This work was supported by the 973 program under Grant No. 2011CBA00112, by the NSF of China under Grant Nos. 10874215, 10934008, and 11034012, by the Fundamental Research Funds for Central Universities, and by the Research Funds of RUC.

Note added in proof: after completion of this manuscript, we became aware of neutron diffraction results from the group of W. Bao.³⁷ In exact analogy with our measurements, the magnetic Bragg peak intensities show a rapid downturn as the temperature is lowered below T_c , confirming the strong competition between the magnetic and superconducting order parameters.

-
- ¹ J. G. Guo, S. F. Jin, G. Wang, S. C. Wang, K. X. Zhu, T. T. Zhou, M. He, and X. L. Chen, Phys. Rev. **82**, 180520(R) (2010).
- ² A. Krzton-Maziopa, Z. Shermadini, E. Pomjakushina, V. Pomjakushin, M. Bendele, A. Amato, R. Khasanov, H. Luetkens and K. Conder, J. Phys.: Condens. Matter **23**, 052203 (2011); Y. Mizuguchi, H. Takeya, Y. Kawasaki, T. Ozaki, S. Tsuda, T. Yamaguchi, and Y. Takano, Appl. Phys. Lett. **98**, 042511(2011); A. F. Wang, J. J. Ying, Y. J. Yan, R. H. Liu, X. G. Luo, Z. Y. Li, X. F. Wang, M. Zhang, G. J. Ye, P. Cheng, Z. J. Xiang, and X. H. Chen, Phys. Rev. B **83**, 060512(2011); M. H. Fang, H. D. Wang, C. H. Dong, Z. J. Li, C. M. Feng, J. Chen and H. Q. Yuan, Europhys. Lett. **94**, 27009 (2011).
- ³ Z. Wang, Y. J. Song, H. L. Shi, Z.W. Wang, Z.Chen, H. F. Tian, G. F. Chen, J. G. Guo, H. X. Yang, J. Q. Li, Phys. Rev. B **83**, 140505(R) (2011).
- ⁴ P. Zavalij, Wei Bao, X. F. Wang, J. J. Ying, X. H. Chen, D. M. Wang, J. B. He, X. Q. Wang, G.F. Chen, P-Y Hsieh, Q. Huang, M. A. Green, Phys. Rev. B **83**, 132509 (2011).
- ⁵ Z. G. Chen, R. H. Yuan, T. Dong, G. Xu, Y. G. Shi, P. Zheng, J. L. Luo, J. G. Guo, X. L. Chen, N. L. Wang, Phys. Rev. B **83**, 220507(R) (2011).
- ⁶ A. M. Zhang, K. Liu, J. H. Xiao, J. B. He, D. M. Wang, G. F. Chen, B. Normand, and Q. M. Zhang, Phys. Rev. B **85**, 024518 (2012).
- ⁷ A. P. Litvinchuk, V. G. Hadjiev, M. N. Iliev, Bing Lv, A. M. Guloy, and C. W. Chu, Phys. Rev. B **78**, 060503 (2008).
- ⁸ T.-L. Xia, D. Hou, S. C. Zhao, A. M. Zhang, G. F. Chen, J. L. Luo, N. L. Wang, J. H. Wei, Z.-Y. Lu, and Q. M. Zhang, Phys. Rev. B **79**, 140510(R) (2009).
- ⁹ A. M. Zhang, K. Liu, J. H. Xiao, J. B. He, D. M. Wang, G. F. Chen, B. Normand, Q. M. Zhang, unpublished (arXiv:1105.1198).
- ¹⁰ W. Bao, Q. Huang, G. F. Chen, M. A. Green, D. M. Wang, J. B. He, X. Q. Wang, and Y. Qiu, Chin. Phys. Lett. **28**, 086104 (2011); F. Ye, S. Chi, Wei Bao, X. F. Wang, J. J. Ying, X. H. Chen, H. D. Wang, C. H. Dong, and M. H. Fang, Phys. Rev. Lett **107**, 137003 (2011).
- ¹¹ Wei Bao, G. N. Li, Q. Huang, G. F. Chen, J. B. He, M. A. Green, Y. Qiu, D. M. Wang, and J. L. Luo, unpublished (arXiv:1102.3674).
- ¹² V. Yu. Pomjakushin, D. V. Sheptyakov, E. Pomjakushina, A. Krzton-Maziopa, K. Conder, D. Chernyshov, V. Svitlyk, and Z. Shermadini, Phys. Rev. B **83**, 144410 (2011); M. Wang, M. Wang, G. Li, Q. Huang, C. Li, G. Tan, C. Zhang, H. Cao, W. Tian, Y. Zhao, Y. Chen, X. Lu, B. Sheng, H. Luo, S. Li, M. Fang, J. Zarestky, W. Ratchiff, M. Lumsden, J. Lynn, and P. Dai, Phys. Rev. B **84**, 094504 (2011); W. Li, H. Ding, P. Deng, K. Chang, C. L. Song, K. He, L. L. Wang, X. C. Ma, J. P. Hu, X. Chen, and Q. K. Xue, Nature Physics **8**, 126 (2012); P. Cai, C. Ye, W. Ruan, X. D. Zhou, A. F. Wang, M. Zhang, X. H. Chen, and Y. Y. Wang, Phys. Rev. B **85**, 094512 (2012).
- ¹³ R. H. Liu, X. G. Luo, M. Zhang, A. F. Wang, J. J. Ying, X. F. Wang, Y. J. Yan, Z. J. Xiang, P. Cheng, G. J. Ye, Z. Y. Li, X. H. Chen, Europhys. Lett. **94**, 27008 (2011).
- ¹⁴ D .H. Ryan, W. N. Rowan-Weetaluktuk, J. M. Cadogan, R. Hu, W. E. Straszheim, S. L. Bud'ko, P. C. Canfield, Phys. Rev. B. **83**, 104526 (2011); Z. W. Li, X. M. Ma, H. Pang, and F. S. Li, Chin. Phys. B **21**, 047601 (2012).
- ¹⁵ Z. Shermadini, A. Krzton-Maziopa, M. Bendele, R. Khasanov, H. Luetkens, K. Conder, E. Pomjakushina, S. Weyeneth, V. Pomjakushin, O. Bossen, and A. Amato, Phys. Rev. Lett. **106**, 117602 (2011).
- ¹⁶ M. Y. Wang, C. Fang, D. X. Yao, G. T. Tan, L. W. Harriger, Y. Song, T. Netherton, C. L. Zhang, M. Wang, M. B. Stone, W. Tian, J. P. Hu, P. C. Dai, Nature Communications **2**, 580 (2011).
- ¹⁷ W. Q. Yu, L. Ma, J. B. He, D. M. Wang, T.-L. Xia, G. F. Chen, and W. Bao, Phys. Rev. Lett. **106**, 197001 (2011).
- ¹⁸ T. Qian, X. P. Wang, W. C. Jin, P. Zhang, P. Richard, G. Xu, X. Dai, Z. Fang, J. G. Guo, X. L. Chen, and H. Ding, Phys. Rev. Lett. **106**, 187001 (2011); Y. Zhang, L.

- X. Yang, M. Xu, Z. R. Ye, F. Chen, C. He, H. C. Xu, J. Jiang, B. P. Xie, J. J. Ying, X. F. Wang, X. H. Chen, J. P. Hu, M. Matsunami, S. Kimura, and D. L. Feng, *Nat. Mater.*, **10**, 273 (2011); D. X. Mou, S. Y. Liu, X. W. Jia, J. F. He, Y. Y. Peng, L. Zhao, L. Yu, G. D. Liu, S. L. He, X. L. Dong, J. Zhang, H. D. Wang, C. H. Dong, M. H. Fang, X. Y. Wang, Q. J. Peng, Z. M. Wang, S. J. Zhang, F. Yang, Z. Y. Xu, C. T. Chen, and X. J. Zhou, *Phys. Rev. Lett.* **106**, 107001 (2011).
- ¹⁹ A. Charnukha, J. Deisenhofer, D. Pröpper, M. Schmidt, Z. Wang, Y. Goncharov, A. N. Yaresko, V. Tsurkan, B. Keimer, A. Loidl, and A. V. Boris, *Phys. Rev. B* **85**, 100504(R) (2012).
- ²⁰ F. Chen, M. Xu, Q. Q. Ge, Y. Zhang, Z. R. Ye, L. X. Yang, J. Jiang, B. P. Xie, R. C. Che, M. Zhang, A. F. Wang, X. H. Chen, D. W. Shen, J. P. Hu, and D. L. Feng, *Phys. Rev. X* **1**, 021020 (2011).
- ²¹ V. Ksenofontov, G. Wortmann, S. A. Medvedev, V. Tsurkan, J. Deisenhofer, A. Loidl, and C. Felser, *Phys. Rev. B* **84**, 180508(R) (2011).
- ²² A. Ricci, N. Poccia, G. Campi, B. Joseph, G. Arrighetti, L. Barba, M. Reynolds, M. Burghammer, H. Takeya, Y. Mizuguchi, Y. Takano, M. Colapietro, N. L. Saini, and A. Bianconi, *Phys. Rev. B* **84**, 060511(R) (2011).
- ²³ R. H. Yuan, T. Dong, Y. J. Song, P. Zheng, G. F. Chen, J. P. Hu, J. Q. Li, and N. L. Wang, *Sci. Rep.* **2**, 221 (2012).
- ²⁴ W. Li, H. Ding, P. Deng, K. Chang, C. L. Song, K. He, L. L. Wang, X. C. Ma, J. P. Hu, X. Chen, and Q. K. Xue, *Nature Phys.* **8**, 126 (2012).
- ²⁵ G. Friemel, J. T. Park, T. A. Maier, V. Tsurkan, Y. Li, J. Deisenhofer, H.-A. Krug von Nidda, A. Loidl, A. Ivanov, B. Keimer, and D. S. Inosov, *Phys. Rev. B* **85**, 140511(R) (2012).
- ²⁶ D. M. Wang, J. B. He, T.-L. Xia, and G. F. Chen, *Phys. Rev. B* **83**, 132502 (2011).
- ²⁷ P. A. Fleury and H. J. Guggenheim, *Phys. Rev. Lett.* **24**, 1346 (1970).
- ²⁸ T. P. Devereaux, and R. Hackl, *Rev. Mod. Phys.* **79**, 179 (2007) and references therein.
- ²⁹ K. Okazaki, S. Sugai, S. Niitaka, and H. Takagi, *Phys. Rev. B* **83**, 035103 (2011); S. Sugai, Y. Mizuno, R. Watanabe, T. Kawaguchi, K. Takenaka, H. Ikuta, Y. Takayanagi, N. Hayamizu, Y. Sone, unpublished (arXiv:1010.6151).
- ³⁰ S. Sugai, S. Shamoto, and M. Sato, *Phys. Rev. B* **38**, 6436 (1988).
- ³¹ C.-C. Chen, C. J. Jia, A. F. Kemper, R. R. P. Singh, and T. P. Devereaux, *Phys. Rev. Lett.* **106**, 067002 (2011).
- ³² Y. Z. You, H. Yao, and D.-H. Lee, *Phys. Rev. B* **84**, 020406 (2011).
- ³³ J. Lorenzana and G. A. Sawatzky, *Phys. Rev. Lett.* **74**, 1867 (1995); *Phys. Rev. B* **52**, 9576 (1995).
- ³⁴ P. J. Freitas and R. R. P. Singh, *Phys. Rev. B* **62**, 5525 (2000).
- ³⁵ G. Blumberg, Moonsoo Kang, M. V. Klein, K. Kadowaki, C. Kendziora, *Science* **278**, 1427 (1997).
- ³⁶ X. W. Yan, M. Gao, Z. Y. Lu, and T. Xiang, *Phys. Rev. B* **83**, 233205 (2011).
- ³⁷ W. Bao, private communication.